LATERAL BUCKLING PROBLEM: MODIFICATIONS OF STANDARD GFRP SECTIONS SHAPE AND PROPORTIONS

Francesco ASCIONE
PhD, Assistant Professor
Department of Civil Engineering, University of Salerno, Italy
Via Giovanni Paolo II, 132, Fisciano (SA)
*fascione@unisa.it**

Marco LAMBERTI
PhD Student
Department of Civil Engineering, University of Salerno, Italy
Via Giovanni Paolo II, 132, Fisciano (SA)
malamberti@unisa.it

Ghani RAZAQPUR
Full Professor
Department of Civil Engineering, McMaster University, Canada
1280 Main Street W. Hamilton, ON L8S 4L7
razaqpu@mcmaster.ca

Abstract

In this paper the first results of a comprehensive numerical investigation regarding the flexural–torsional response of pultruded slender beams is presented. The goal of the research is to propose GFRP standard cross-sections of such proportions and shapes that would possess improved strength, stability and deformational characteristics compared to the corresponding existing sections whose proportions are generally based on standard steel sections. As GFRP sections are thin-walled but are significantly less stiff than similar steel sections, the study focuses on enhancing their appropriate stiffness and buckling strength. The novel and efficient numerical model used in this investigation was developed by the writers and can be used to trace the complete pre-buckling geometrically nonlinear response of any GFRP or steel thin-walled member with open or closed cross-section. The bucking load is computed by the asymptotic value of the load-displacement curve. It is demonstrated that due to their unsuitable proportions, available standard GFRP sections do not have adequate stiffness and buckling strength. Consequently, relative to T-cross section only recommendations are made for new sectional proportions and modified shape. The superiority of the proposed section is quantified by an efficiency factor, defined in terms of ratio of strength gain to material volume increase.

Keywords: Analysis, bending, buckling, cross-section, fibre-reinforced polymer and torsion.

1. Introduction

Historically, Fibre-Reinforced-Polymer (FRP) pultruded profiles were designed by the pultrusion industry and were intended for low-stress applications (cooling towers, water and waste-water treatment plants, etc.), taking into account their principal features such as their high stiffness and strength-to-weight ratio, magnetic transparency, corrosion resistance, and an effective manufacturing process. However, since the late nineties, FRP pultruded profiles reinforced with glass fibres (GFRP) have been used in civil engineering as primary structural members, complementing other conventional materials such as steel, concrete, and wood in pedestrian and highway bridges, railway lines ([1]-[3]), and in the construction of full-composite structures. One of the first, as well as one of the most famous, full-composite structures was the five-storey GFRP Eyecatcher Building erected in Basel, Switzerland in 1998 for the Swiss Building Fair. It is also the tallest FRP structure constructed until now.
In order to make pultruded members more appealing to the construction industry, most manufacturers produce profiles that imitate standard structural steel members (e.g. I-, H-, C-,

and angle profiles), but in the field of composite research, the belief that these "steel-like" profiles do not represent the optimum geometry for composite sections is gradually gaining currency. Considering that standard engineering guidelines developed for conventional materials are not applicable to FRP shapes, several technical documents dealing with the design equations and methods, material properties, and safety factors for pultruded elements have been developed or under development [4] -[7].

In these documents it is specified that the pultruded elements could be considered as linear elastic, homogeneous, and transversely isotropic in the case of aligned fibres, with the plane of isotropy being normal to the longitudinal axis (i.e. the axis of pultrusion). Their mechanical behaviour is strongly affected by warping strains as well as shear deformations, which, coupled with the time-dependent nature of these materials, govern their complex mechanical behaviour.

The lateral buckling behaviour of FRP beams has been widely investigated in the literature from the theoretical, numerical, and experimental points of view. Recent experimental studies by Mosallam et al. [8] and Feo et al. [9] showed that for composite pultruded beams the hypothesis of rigid web–flange junctions, or connections, need to be changed, primarily due to the anisotropy of the constitutive behaviour of the material, but also due to the higher local resin concentration at the web–flange junctions, which is believed to reduce the flexural rigidity of the cross-section.

Based on the latter finding, the writers developed an innovative mechanical model to predict the nonlinear pre-buckling behaviour of generic composite beams with open or closed cross section [10]-[12], taking into account the deformability of the connections joining the panels or plates that form the cross-section. The main assumption is that the cross section be viewed as an assemblage of thin rectangular elements connected to each other at their ends.

The aim of the present paper is to identify, via detailed analysis, appropriate geometric parameters for GFRP T- section only that can be judiciously selected to improve its overall resistance, stability and serviceability when subjected to flexural–torsional actions. The improvements can be judged by comparing the response of the GFRP section with enhanced properties to those of similar existing section available commercially.

2. Main features of the proposed mechanical model

The main idea is that typically the cross section of a thin-walled member is composed of a defined number of thin rectangular panels mutually interconnected at a defined number of internal points or nodes (internal connections), as illustrated in Figure 1. Each panel is assumed to be thin and is modelled using a full second-order deformable beam theory, accounting for both the warping effects and possible displacement discontinuities at the connections of each panel with the adjoining panels. Furthermore, the hypothesis of small strain and moderate rotation is adopted in the formulation.

In view of the above assumptions, the displacement field of each panel is given by

$$u^{(i)}(x,y,z) = u_o^{(i)}(z) - \varphi_3^{(i)}(z)\left(y - y_o^{(i)}\right) \tag{1.a}$$

$$v^{(i)}(x,y,z) = v_o^{(i)}(z) + \varphi_3^{(i)}(z)\left(x - x_0^{(i)}\right) \tag{1.b}$$

$$w^{(i)}(x,y,z) = \bar{w}_h^{(i)}(z)\, f_h^{(i)}(s) - \varphi_s^{(i)}(z)\, n \tag{1.c}$$

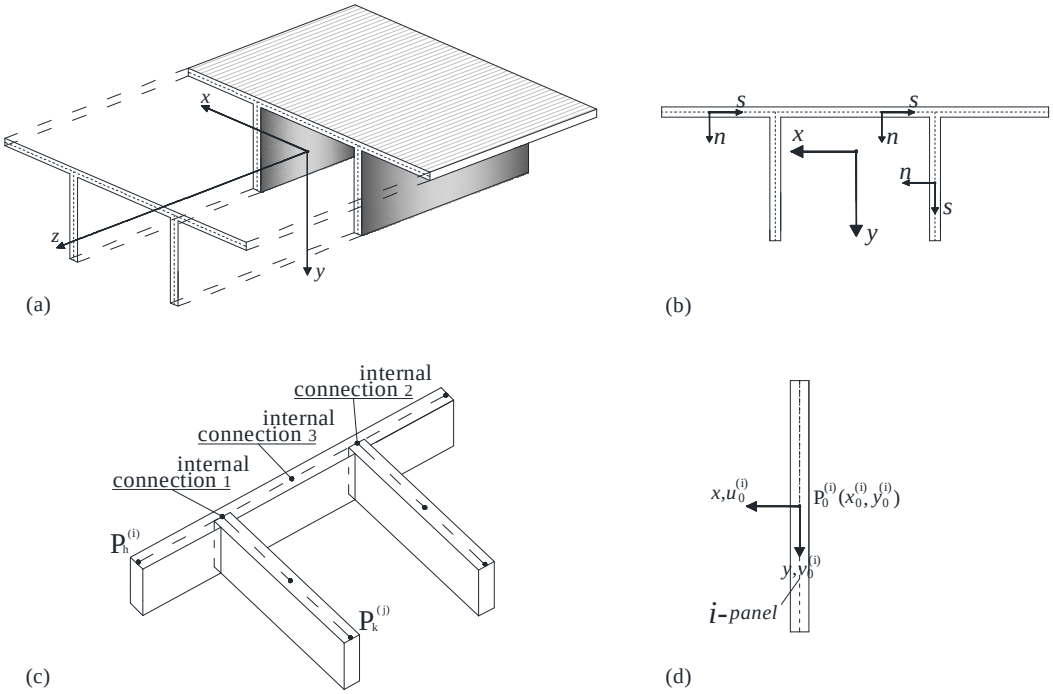

Figure 1. (a) Typical beam; (b) cross section; (c) positions of the internal connections; (d) generic *i*-panel.

In Eqs. (1.a–1.c) the quantities $u_o^{(i)}$ and $v_o^{(i)}$ represent the out-of-plane and in-plane displacement components of the point $P_o^{(i)} \equiv \left(x_0^{(i)}, y_0^{(i)}\right)$ along the *x* and *y* axes, respectively (Figure 1d) and $\varphi_3^{(i)}$ denotes the twisting rotation of the panel. The latter point usually coincides with the centroid of the panel. In Eq. (1.c) the displacement component $w^{(i)}$ (axial or lengthwise panel displacement) is modelled as the sum of two parts: the first is a linear combination of the kinematic unknowns, $\overline{w}_h^{(i)}$, which represent the axial displacements of the points, $P_h^{(i)}$, lying on the mid-line of the panel, and having interpolating polynomials $f_h^{(i)}$; the second is displacement due to flexural rotation, $\varphi_s^{(i)}$, about the normal, *n*, to the mid-line of the panel. Note that the polynomials $f_h^{(i)}$ are functions of the coordinate *s* running along the middle line of the panel.

In [12] it was shown that in order to adequately simulate the warping behaviour of the cross-section, the polynomials $f_h^{(i)}$ must be at least quadratic, which requires three points or nodes along each panel cross-section in order to determine the coefficients of the quadratic function. Accordingly, one node is located at each end of the panel and a third one is placed at its mid point. These nodes are denoted by $P_1^{(i)}$, $P_3^{(i)}$, $P_2^{(i)}$, respectively, in Figure 2.

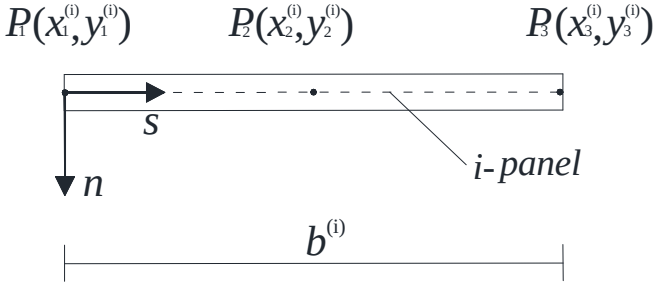

Figure 2. Generic *i*-panel.

Based on the above, the warping displacement is written as follows:

$$\bar{w}_h^{(i)}(z)\, f_h^{(i)}(s) = \bar{w}_1^{(i)}(z)\, f_1^{(i)}(s) + \bar{w}_2^{(i)}(z)\, f_2^{(i)}(s) + \bar{w}_3^{(i)}(z)\, f_3^{(i)}(s) \tag{2}$$

where $\bar{w}_h^{(i)}\,(h=1,2,3)$ represent the tangential displacements at nodes $P_h^{(i)}$ while $f_h^{(i)}$ (h=1,2,3) are expressed as follows:

$$f_1^{(i)} = 1 + a_1^{(i)} s + b_1^{(i)} s^2 \tag{3.a}$$
$$f_2^{(i)} = a_2^{(i)} s + b_2^{(i)} s^2 \tag{3.b}$$
$$f_3^{(i)} = a_3^{(i)} s + b_3^{(i)} s^2 \tag{3.c}$$

In Eqs. (3.a–c) the coefficients of the polynomials terms are given by:

$$a_1^{(i)} = \frac{\left(s_2^{(i)}\right)^2 - \left(s_3^{(i)}\right)^2}{\Delta},\ b_1^{(i)} = \frac{s_3^{(i)} - s_2^{(i)}}{\Delta},\ a_2^{(i)} = \frac{\left(s_3^{(i)}\right)^2}{\Delta},\ b_2^{(i)} = -\frac{s_3^{(i)}}{\Delta},\ a_3^{(i)} = -\frac{\left(s_2^{(i)}\right)^2}{\Delta},$$
$$b_3^{(i)} = \frac{s_2^{(i)}}{\Delta},\ \Delta = s_2^{(i)}\left(s_3^{(i)}\right)^2 - s_3^{(i)}\left(s_2^{(i)}\right)^2 \cdot \tag{4.a-g}$$

In Eqs. (4.a–g) the symbols $s_2^{(i)}$ and $s_3^{(i)}$ are the tangential displacements of nodes $P_2^{(i)}$ and $P_3^{(i)}$, respectively.

2.2 Internal connections

The internal connections of the panels are modelled by means of four nonlinear continuously distributed springs, which can capture the relative translational and rotational movements at the connections of adjoining panels. The generalized force-displacement relationship of the springs is illustrated in Figure 3. The symbols in this figure are defined with reference to the cross-sections in Figure 2 as follows:

- σ is the generalized force or action, which, depending on the spring considered, represents the web–flange force per unit area along the *x*-axis (σ_u), the *y*-axis (σ_v), and the *z*-axis (σ_w), or the web–flange torsional moment per unit length around the *z*-axis (μ_3);
- d is the displacement discontinuity associated with the generalized force σ; it represents the web–flange relative displacement along the *x*-axis (d_u), the *y*-axis (d_v), and the *z*-axis (d_w), or the web–flange relative twist around the *z*-axis (d_{φ_3});
- σ_y and σ_u are, respectively, the maximum elastic and ultimate values of the considered web–flange forces;
- d_y and d_u are , respectively, the maximum elastic and ultimate values of the relative displacement associated with generalized force being considered;
- K_1 and K_2 are , respectively, the elastic and post-elastic stiffness constants of the springs. Mosallam et al. [9] have shown an innovative procedure for how to determine these constants experimentally.

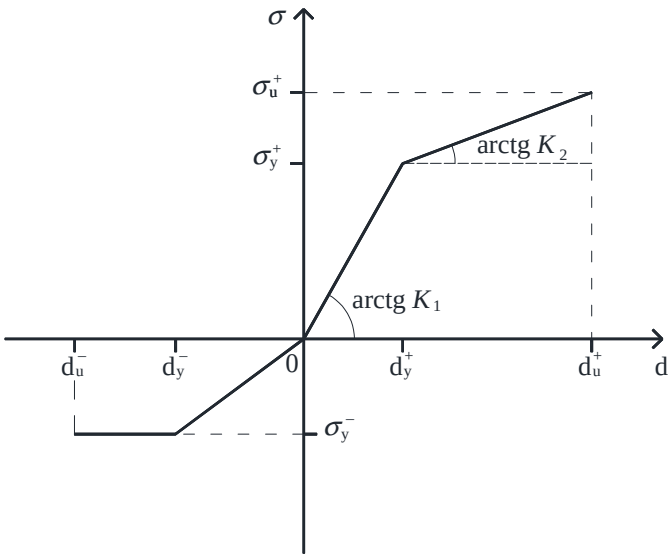

Figure 3. Generic relationship between web–flange relative displacement, d, and the associate generalized force σ.

2.3 Stress–strain relationship

Assuming linear elasticity, the Second Piola–Kirchhoff stress tensor and the Green strain tensor for each panel are related as:

$$\left[S_{13},\, S_{23},\, S_{33}\right]^T = \begin{bmatrix} G_{13} & 0 & 0 \\ 0 & G_{23} & 0 \\ 0 & 0 & E_L \end{bmatrix} \left[2E_{13},\, 2\mathrm{E}_{23},\, \mathrm{E}_{33}\right]^T \tag{5}$$

In Eq. (5), symbols E_L, G_{13}, and G_{23} denote, respectively, Young's modulus along the member axis and the shear moduli within the (x–z) and (y–z) planes (Figure 1). Strain components E_{13}, E_{23}, and E_{33}, the only non-zero components of the Green–Lagrange strain tensor, are expressed as

$$E_{13} \cong \frac{1}{2}\left[u_0'^{(i)} - \varphi_3'^{(i)}\left(y - y_o^{(i)}\right) + \bar{w}_h^{(i)} g_{1,h}^{(i)} - \varphi_s^{(i)}\frac{dn}{dx}\right] + \frac{1}{2}\left[v_0'^{(i)}\varphi_3^{(i)} + \varphi_3^{(i)}\varphi_3'^{(i)}\left(x - x_o^{(i)}\right) + \bar{w}_h^{(i)}\bar{w}_k'^{(i)}\, g_{1,h}^{(i)}\, g_{3,k}^{(i)}\right] \tag{6.a}$$

$$E_{23} \cong \frac{1}{2}\left[v_0'^{(i)} + \varphi_3'^{(i)}\left(x - x_o^{(i)}\right) + \bar{w}_h^{(i)} g_{2,h}^{(i)} - \varphi_s^{(i)}\frac{dn}{dy}\right] + \frac{1}{2}\left[-u_0'^{(i)}\varphi_3^{(i)} + \varphi_3^{(i)}\varphi_3'^{(i)}\left(y - y_o^{(i)}\right) + \bar{w}_h^{(i)}\bar{w}_k'^{(i)} g_{2,h}^{(i)}\, g_{3,k}^{(i)}\right] \tag{6.b}$$

$$\begin{aligned} E_{33} \cong{}& \left[\bar{w}_h'^{(i)} g_{3,h}^{(i)} - \varphi_s'^{(i)} n\right] + \frac{1}{2}\left\{\left(u_0'^{(i)}\right)^2 + \left(v_0'^{(i)}\right)^2 + \left(\varphi_3'^{(i)}\right)^2\left[\left(x - x_o^{(i)}\right)^2 + \left(y - y_o^{(i)}\right)^2\right] + \right. \\ & \left. -2u_0'^{(i)}\varphi_3'^{(i)}\left(y - y_o^{(i)}\right) + 2v_0'^{(i)}\varphi_3'^{(i)}\left(x - x_o^{(i)}\right) + \left(\bar{w}_h'^{(i)} g_{3,h}^{(i)}\right)^2 + \left(1 - \delta_{hk}\right)\bar{w}_h'^{(i)}\bar{w}_k'^{(i)} g_{3,h}^{(i)}\, g_{3,k}^{(i)}\right\} \end{aligned} \tag{6.c}$$

where functions $g_{1,h}^{(i)}(s)$, $g_{2,h}^{(i)}(s)$, and $g_{3,h}^{(i)}(s)$ have the form

$$g_{1,h}^{(i)}(s) = \frac{\partial f_h^{(i)}}{\partial x} = a_h^{(i)}\frac{ds}{dx} + 2b_h^{(i)}\frac{ds}{dx} \tag{7.a}$$

$$g_{2,h}^{(i)}(s) = \frac{\partial f_h^{(i)}}{\partial y} = a_h^{(i)}\frac{ds}{dy} + 2b_h^{(i)}\frac{ds}{dy} \tag{7.b}$$

$$g_{3,h}^{(i)}(s) = f_h^{(i)}(s) \tag{7.c}$$

It is worth pointing out that despite the expectation that E_{13}, E_{23}, and E_{33} being the only non-zero strain components, it emerges that E_{11}, E_{12}, and E_{22} are also not zero. This is due to the simplified form of the displacement field. The simplified kinematic relationships adopted in Eq. (1) were evaluated as appropriate for practical purposes. However, as demonstrated later, the strain E_{11}, E_{12}, and E_{22} can be ignored without loss of accuracy.

2.4 Variational formulation

For formulating the finite element model necessary to perform numerical analysis, the equilibrium problem was recast using the principle of virtual displacement as follows:

$$\delta L_{\text{int}} + \delta L_{\text{con}} = \delta L_{ext} \tag{8}$$

The symbols δL_{int}, δL_{con} and δL_{ext} represent the virtual work of internal stresses that accounts for second-order terms, the work done by internal connections, and the work done by the external forces, respectively.

Longitudinally the member is modelled by a two node finite element with cubic Hermitian shape functions. More details of the formulation, including the expressions for the generalised displacement, stress, and strain fields, are given in [12]. The reliability and accuracy of the proposed numerical model are also demonstrated in the latter reference.

3. Numerical results

The aim is to analyse the response of a T- members having the common cross-sectional shapes available on the market, and to recommend typical changes to its proportions or shape, with the goal of enhancing its strength, stiffness and/or stability. Based on the results of the presented analyses, improved cross-sectional proportions or alternative efficient modified shapes are proposed. It should be pointed out that the stability of a thin-walled section depends on a large number of material and geometric properties, and loading configuration of the member. The geometric properties include the section torsional, polar, and warping constants as well as its cross-sectional area, second moments of area, and the member unsupported length. These parameters cannot be optimized for every loading and geometric scenario using only one section type or proportions; nevertheless, it is possible, as shown in this investigation, to significantly improve their resistance by judicious choices of section shape and proportions.

T- cross section member with cantilever support conditions is investigated. The member is subjected to eccentrically applied concentrated load as shown in Figure 4. The mechanical properties of the analyzed steel and GFRP sections are reported in Table 1, while the geometric characteristics of each cross section are summarised in Table 2, and the symbols in Table 2 are identified in Figure 4. For simplicity, the member length is taken as 3000 mm for all the investigated cases.

In each case the member is discretized by a mesh comprising 500 two-node finite elements. As demonstrated in [12], this mesh is deemed satisfactory for the purpose of the current analyses.

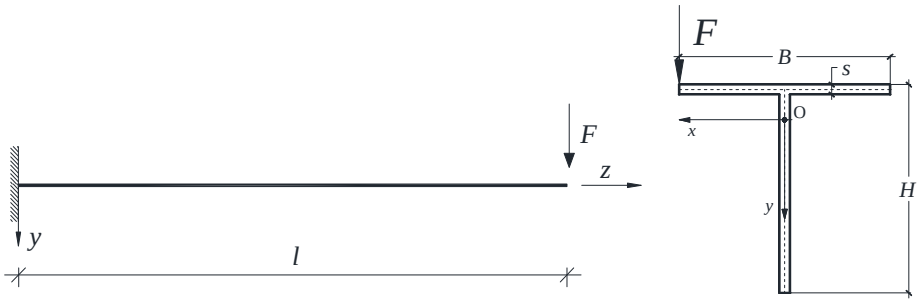

Figure 4. Geometry, loading and boundary conditions investigated.

Table 1. Steel and GFRP mechanical properties

Steel mechanical properties			
Young's modulus of elasticity	E	MPa	210,000
Shear modulus of elasticity	G	MPa	81,000
Yield strength	f_y	MPa	275
Ultimate strength	f_u	MPa	430
GFRP mechanical properties			
Young's modulus of elasticity(*)	$E_{0°}$	MPa	23,000
Shear modulus of elasticity	G_{xz}, G_{yz}	MPa	3,000
Flexural strength(*)	$f_{b,0°}$	MPa	240
Tensile strength(*)	$f_{t,0°}$	MPa	240
Compressive strength(*)	$f_{c,0°}$	MPa	240
Shear strength	f_τ	MPa	25

(*) pulling direction during pultrusion process (axis of pultrusion)

Table 2. Cross section shapes and relative geometrical parameters

Cross section shape	T		
Geometrical dimensions		measure unit	value
Flange panel width	B	mm	80.0
Flange panel thickness	s	mm	9.0
Web panel thickness	s	mm	9.0
Whole cross section height	H	mm	80

The results for the cantilever beam-columns, including the magnitude of the critical applied load, F_{crit}, are reported in Table 3. The table lists the selected commercially available standard steel and GFRP sections and their dimensions, followed by a number of analogous GFRP shapes with modified dimensions, and finally a similar but more efficient shape proposed based on the results of the current analyses. The standard sections are simply termed Steel and GFRP while the modified GFRP sections are dubbed "GFRP*i*". Note, in the table for each cross section the dimensions that are altered, compared to the corresponding standard section dimensions, are underlined. Finally, in each case the ratios of the volume and critical load of each modified section to the volume and critical load of the corresponding standard section are computed and shown in columns 5 and 4 of Table 3. Section efficiency factor η, defined as the ratio of increase in volume to increase in critical load, is indicated in the last column of

the table. Note that η values greater than one indicate more efficient section than the corresponding standard section.

Table 3 – Cantilever beam-columns: cross sectional shape, dimensions and relative buckling loads

Case studied	Cross-section Dimensions [mm]		Load^{crit}	$L^{crit}_{GFRPi} / L^{crit}_{GFRP}$	V_{GFRPi} / V_{GFRP}	η
		(H x B x s)	**F^{crit} [kN]**	**[-]**	**[-]**	**[-]**
(T-section)	Steel	(80 x 80 x 9)	2.40	-	-	-
	GFRP	(80 x 80 x 9)	0.34	1.00	1.00	1.00
	GFRP*1*	(80 x 80 x 18)	0.65	1.91	1.88	1.02
	GFRP*2*	(160 x 80 x 9)	0.40	1.17	2.94	0.40
	GFRP*3*	(80 x 80 x 27)	0.90	2.65	2.64	1.00
	GFRP*4*	(120 x 80 x 13.5)	0.80	2.35	1.85	1.27
	GFRP*5*	(80x 120 x 9)	0.40	1.17	1.26	0.92
	GFRP*6*	(80 x 120 x 13.5)	0.80	2.35	1.85	1.27
	GFRP*7*	(proposed new shape, see Figure 5)	1.80	5.29	3.22	1.64

In Figures 5 the load versus displacement curves are reported. In Figure 5a the applied load *F*-lateral displacement, *u*, curve for point P on the flange, and in Figure 5b the load *F*-vertical displacement, *v*, curve for point O on the web are plotted. The above displacements are at the free end of the cantilever.

Notice the nearly fivefold increase in F_{crit} and the threefold increase in stiffness of the proposed new T-shape compared to the standard section. The new section uses approximately three times more material than the standard section but has over five times higher critical load, with η=1.64.

The modified section GFRP4 uses instead two times more material than the standard section but has two times higher critical load, hence its η=1.27. Furthermore, compared to modified section GFRP4, the proposed section contains 74% more material, but its critical load is 225% higher. In fact, it is worth noting that F_{crit} for the new shape is 75% of the critical load of the companion steel section while F_{crit} for the GFRP4 shape is 33% of that of steel section.

This is possible because the new cross section presents an innovative shape where the torsional and flexural stiffness are both increased in a balanced manner. Note that Figure 5a and 5b may be also used to examine the effects of certain changes in the standard T-section dimensions on its deformation, stiffness and stability.

It is worth noting that compared to the standard steel section, in each case the worst response, in terms of strength and stiffness, is exhibited by the companion standard GFRP section, which supports the argument that the current commercially available GFRP sections are not properly shaped or proportioned, at least from the perspective of lateral-torsional stability.

If the intent of the current selection of GFRP standard sections is to mimic analogous steel sections, they fall dramatically short of having comparable performance insofar as buckling strength and stiffness are concerned.

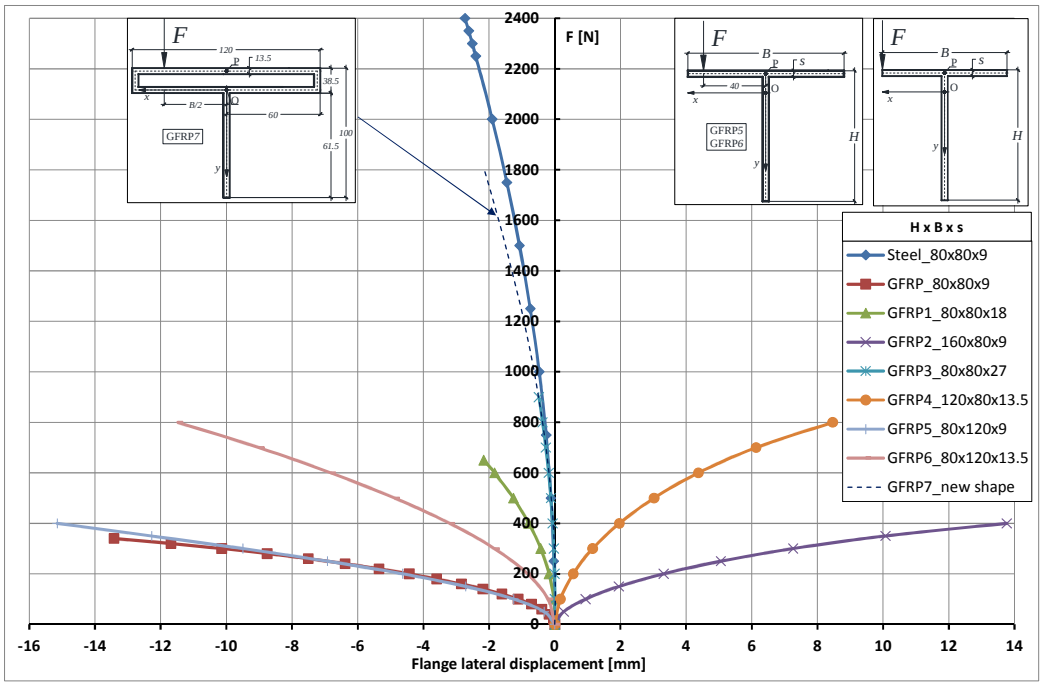

Figure 5a. Case A1 – Load *F* versus lateral displacement, *u*, at point P on the flange

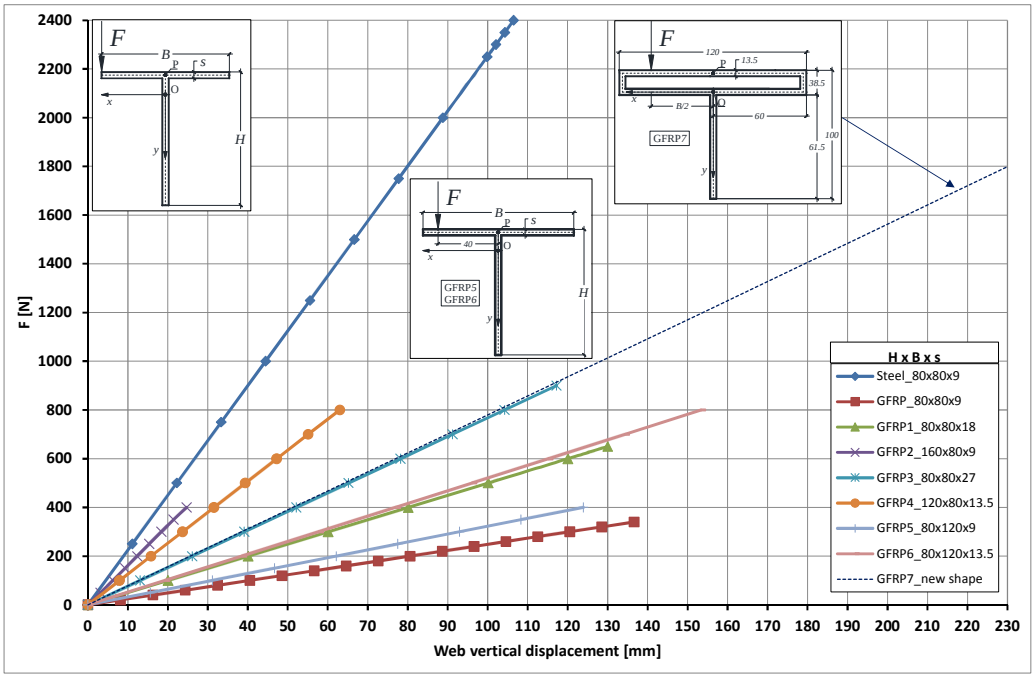

Figure 5b. Case A1 – Load *F* versus vertical displacements, *v*, at point O on the web

For example, the numerical results presented in Figures 5 show that in the case of the T-cross section, deformation control is governed by the vertical displacement *v*, which appears to be about 10 times higher than the horizontal displacement *u*. The global buckling is instead governed, as expected, by the second moment of area about the minor axis of bending. Thus, the numerical results lead one to state that with reference to the standard GFRP T-section:

- increasing thickness, *s*, decreased vertical displacement, *v* , but increased both the buckling load (approximately 165% when *s* is increased threefold) and horizontal displacement, *u*, although the increase in *u* has marginal effect on the deflection limit.

- increasing the width, *B*, 150% increased the buckling load by 17% while neither displacement, *u*, nor and *v* changed significantly;
- increasing the height, *H*, 200% increased the buckling load 17% and reduced the vertical displacement, *v*, dramatically as it approached the corresponding displacement of the companion steel section.

The other modification to the standard cross sectional dimensions investigated in this study involves changes to more than one geometric parameter (*s* and *B*, or *s* and *H*) concurrently, which result in varying degrees of improvement in the section performance as shown in Figures 5. Overall, increasing thickness *s* may be the best choice. Alternatively, if possible, it is advantageous to modify the cross-sectional shape as illustrated by the shape GFRP7 in the current study.

4. Conclusions

In this paper the first results of a comprehensive numerical investigation is performed to analyze the deformations and stability of pultruded slender beams subjected to combined axial–flexural–torsional actions and how changes in the dimensions and shape of their cross-sections affect their stability and stiffness. The overall objective was to identify several GFRP cross section geometries by modifying the current standard GFRP shapes available on the market (i.e. those similar to steel cross section shapes), in order to improve their mechanical behaviour. The section analyzed was pultruded slender T- shapes. Cantilever beam-columns (with torsional restraint at the supports) were analyzed subjected to eccentric gravity concentrated load, producing bending shear and torsion. The numerical analyses were performed using a new numerical model, developed by the authors. The model is capable of predicting the nonlinear pre-buckling behaviour of generic composite beam-columns with open or closed cross-section of arbitrary shape. The numerical results lead to the following general conclusions irrespective of the loading and boundary conditions

- standard GFRP T-section is not a suitable choice for full scale FRP structures; however, increasing the flange thickness thicknesses (e,g. doubling) and making the width of the flange, *B*, and the height, *H*, of the whole cross section equal, increases the buckling load by only 20% but causes noticeable reduction in the relevant deformations;

Part of the goal of this investigation is to initiate discussion about the right shape and proportions of GFRP pultruded cross-sections. We believe that section shapes and dimensions should be selected based on the mechanical properties of FRP and not by mimicking steel sections. Therefore, we hope that this would eventually lead to radical changes and rethinking in the production of pultruded composite sections, giving them their appropriate place within the constellation of structural shapes available to structural designers.

5. References

[1] Hollaway, L.C. Applications of fibre-reinforced polymer composite materials. In ICE manual of construction materials: Polymers and Polymer Fibre Composites. London: Thomas Telford Limited, 2010, 109–127.

[2] Bank, L.C. Composites for Construction—Structural Design with FRP Materials. New Jersey: John Wiley & Sons, 2006.

[3] Halliwell, S.M. Polymer composites in construction, BRE/DETR UK, BR405, Building Research Establishment, UK, 2000.

[4] Eurocomp design code and handbook. Structural design of polymer composites. The European Structural Polymeric Composites Group; 1996. ISBN 0419194509

[5] European Committee for Standardization (CEN). EN 13706: Reinforced plastics composites-specification for pultruded profiles. Part 1: Designation; Part 2: Methods of test and general requirements; Part 3: Specific requirements. Brussels: CEN; 2002

[6] Technical Document CNR-DT 205/2007. Guide for the design and construction of structures made of FRP pultruded elements. Rome: Italian National Research Council (CNR); 2008.

[7] Mosallam, A.S. Design guide for FRP composite connections. Manuals of practice (MOP) 102. American Society of Civil Engineers (ASCE); 2001.

[8] Mosallam, A.S., Elsadek, A.A., Pul, S. Semi-rigid behaviour of web-flange junctions of open-web pultruded composites. Proceedings of the International Conference on FRP Composites 2009, San Francisco, California.

[9] Feo, L., Mosallam, A.S., Penna, R. Mechanical behavior of web-flange junctions of thin-walled pultruded I-profiles: An experimental and numerical evaluation. Composites: Part B (2013), 48: 18–39.

[10] Ascione, F., Mancusi, G. The influence of the web-flange junction stiffness on the mechanical behavior of thin-walled pultruded beams. Composites: Part B (2013), 55: 599–606.

[11] Ascione, F. Influence of initial geometric imperfections in the lateral buckling problem of thin walled pultruded GFRP I-profiles. Composite Structures (2014), 112: 85–99.

[12] Mancusi, G., Ascione, F., Lamberti, M. Pre-buckling behavior of composite beams: A mechanical innovative approach. Composite Structures (2014), 117: 396–410.